ElectriPop: Low-Cost, Shape-Changing Displays Using Electrostatically Inflated Mylar Sheets

Cathy Mengying Fang
mengyinf@alumni.cmu.edu
Carnegie Mellon University
Pittsburgh, USA

Jianzhe Gu
jianzheg@cs.cmu.edu
Carnegie Mellon University
Pittsburgh, USA

Lining Yao
liningy@cs.cmu.edu
Carnegie Mellon University
Pittsburgh, USA

Chris Harrison
chris.harrison@cs.cmu.edu
Carnegie Mellon University
Pittsburgh, USA

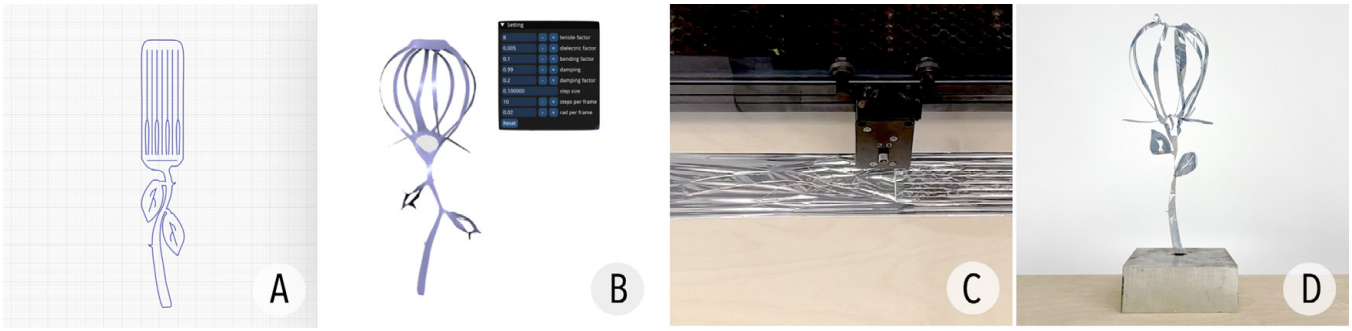

Figure 1: ElectriPop is a shape-changing approach that uses electrostatic forces to "inflate" metalized PET film into complex 3D forms. Our fabrication workflow starts with the user creating a 2D vector illustration of their design (A). As the 2D-to-3D transformation can be complex, we provide a simulation tool that runs in parallel to show the 3D output (B), allowing for rapid iteration. Once satisfied, users proceed to cut the design, e.g., with a laser cutter (C). Users can then place the design on an actuation base (D), which programmatically inflates the form using electrostatic force.

ABSTRACT

We describe how sheets of metalized mylar can be cut and then "inflated" into complex 3D forms with electrostatic charge for use in digitally-controlled, shape-changing displays. This is achieved by placing and nesting various cuts, slits and holes such that mylar elements repel from one another to reach an equilibrium state. Importantly, our technique is compatible with industrial and hobbyist cutting processes, from die and laser cutting to handheld exacto-knives and scissors. Given that mylar film costs <$1 per m^2, we can create self-actuating 3D objects for just a few cents, opening new uses in low-cost consumer goods. We describe a design vocabulary, interactive simulation tool, fabrication guide, and proof-of-concept electrostatic actuation hardware. We detail our technique's performance metrics along with qualitative feedback from a design study. We present numerous examples generated using our pipeline to illustrate the rich creative potential of our method.

CHI '22, April 29-May 5, 2022, New Orleans, LA, USA

ACM ISBN 978-1-4503-9157-3/22/04.
https://doi.org/10.1145/3491102.3501837

CCS CONCEPTS

• **Human-centered computing** → **Displays and imagers**.

KEYWORDS

Shape-changing Interface; Electrostatic Inflation; Computational Fabrication

ACM Reference Format:
Cathy Mengying Fang, Jianzhe Gu, Lining Yao, and Chris Harrison. 2022. ElectriPop: Low-Cost, Shape-Changing Displays Using Electrostatically Inflated Mylar Sheets. In *CHI Conference on Human Factors in Computing Systems (CHI '22), April 29-May 5, 2022, New Orleans, LA, USA.* ACM, New York, NY, USA, 15 pages. https://doi.org/10.1145/3491102.3501837

1 INTRODUCTION

Shape-changing displays offer a uniquely embodied and highly aesthetic mode of computer-human communication, perfect for uses such as ambient displays, embodied avatars, interactive art, and educational experiences. By giving elements form, these applications can become more engaging with increased physicality. However, practical shape-changing displays continue to be elusive, and there is considerable ongoing research in this area, both in the HCI community and beyond. Ideal approaches might be considered to have

the following properties: low-cost, fast-actuating, silent-operation, compact, robust, and easy to fabricate.

In this work we describe ElectriPop, a new fabrication workflow and computational tool that allows sheets of metalized mylar to be cut and then "inflated" into complex 3D forms using electrostatic charge. This is achieved by carefully placing and nesting various cuts, slits, and holes such that mylar elements repel from one another. We provide a brief primer on the principles of our technique's operation. Of course, this introduces interesting design challenges, such as how to assist designers in the creation process given the complex 2D-to-3D transformation process. For this, we developed a simulation tool that runs in parallel with existing vector editing programs that simulates the 3D output. In a design study we conducted, participants found that the real-time visualization greatly facilitated rapid prototyping of forms.

Unlike more exotic shape-changing technologies, our technique involves only a single sheet of thin film, and is compatible with industrial and hobbyist manufacturing processes, including die cutting, laser cutting, vinyl cutting, and even just handheld exacto-knives and scissors. Given that mylar film costs <$1 USD per m^2, this means we can create 3D objects for just a few cents each, opening new uses in consumer objects. In addition to being easy to fabricate and low cost, our technique is also fast-actuating, requires little power to stay inflated, and the operation is nearly silent. We do, however, require an external electrostatic generator to actuate our designs. We built two proof-of-concept actuation bases, both costing under $10 USD. To help illustrate the rich creative potential of our method, we fabricated a series of demos, ranging from popup books to smart speaker avatars. All of our tools and designs are open sourced to bootstrap makers interested in experimenting with our technique.

2 PRINCIPLES OF OPERATION

Electrostatic charge occurs when there is an accumulation or depletion of electrons in a material, giving the object a net negative or positive charge [27]. Unless discharged, this charge is stable (i.e., not flowing), hence the name "static" electricity. Charge can be created in many ways, including mechanically (tribocharging [27], e.g., rubbing your hair with a balloon), chemically (how batteries work), or inductively (e.g., high voltage transformer). As described by Coulomb's law, particles, materials, and objects with like charges repel from one another with an inverse-square distance relationship [22]. We use this repelling force in two distinct ways, for "pop up" and "inflation".

Consider the example in Figure 2. The system is comprised of a conductive base on top of which is taped a piece of conductive film with a small cut (Figure 2A). At rest, this system is neutral, with no imbalance in charge. If we charge the base, the charge will propagate to the whole conductive system (Figure 2B). As the base and film now have the same charge, they will repel; as one side is taped in this example, the film hinges upwards in response to the electrostatic force (Figure 2B, green vector). This is the force we use to "pop up" our designs from a base, overcoming gravity.

The second way we use electrostatic repulsion is to "inflate" our designs. In this simple example, the film has a cut that creates two "arms". When charged, these elements will repel (Figure 2C, green vector), bending and twisting the film, finding an equilibrium between the force pushing them apart and the elasticity of the material resisting the deformation. In more complex 3D examples (like we show later), electrostatic repulsion acts like an inflationary pressure. This behavior to form a minimal energy state is similar to the physics of why bubbles are spherical (surface tension) and balloons are convex (air pressure).

3 RELATED WORK

We now briefly review two main bodies of prior work. In Section 11, after we have described our ElectriPop technique, we provide a comparison to other shape changing technologies.

3.1 2D to 3D transformations & 4D designs

Origami and kirigami, the art of paper folding and cutting respectively, are canonical examples of 2D to 3D shape transformation. Much prior work has leveraged these techniques to create shape-changing interfaces and robots [8, 19, 26, 30, 46, 57]. Researchers from the computer graphics community have also explored computational methods to simulate and design 2D shapes that can be transformed into complex 3D surfaces through e.g., pneumatic actuation [32, 38, 50] or by pre-stretching and releasing fabric [45] or elastic sheets [21, 55].

There is also a large body of work within the HCI community focusing on shape-changing displays that use techniques like pneumatics [23, 41, 43, 54, 65] and fluidics [34, 37, 42]. These systems require air pumps or compressors that are noisy, bulky and power-consuming, and the interfaces themselves involve bladders that are susceptible to puncture. Another common approach are arrays of linear actuators that can change height [5, 13, 51]. These systems are generally expensive, large, immobile, consume significant power, and generate noise during actuation [3].

Other methods leverage physical properties that change materials' structure to achieve shape-change. Some apply different temperatures to shape-memory alloys [9, 55], twisted coil actuators [14], liquid crystal elastomers [2], thermoplastics [4, 20, 61], and other thermo-responsive materials [24, 36, 40]. Others use materials that change their curvature or size under different moisture level [17, 18, 58, 60, 62, 66]. These methods often require complex fabrication processes and the systems have a slow response time [3]. Most related to this work are methods employing electroactive materials. Notable among these are dielectric elastomers (commonly used to create artificial muscles [44]) that use electrostatic forces to compress membranes, which can cause a structure to bend [15] or displace liquid for hydraulic actuation [42].

Uniquely, our shape-changing technique is based on a single homogeneous sheet of low-cost material (mylar film). Further, the electrostatic repulsion forces we use have very fast actuation speeds and essentially-silent operation. Our approach is both accessible to makers and compatible with mass production techniques, which is also uncommon. In section 11, we lay out a detailed comparison of Electripop to other shape-changing methods.

3.2 Electrostatic Inflation

We are not the first to explore using electrostatic forces to inflate mylar structures. Owing to their extraordinary weight-to-volume

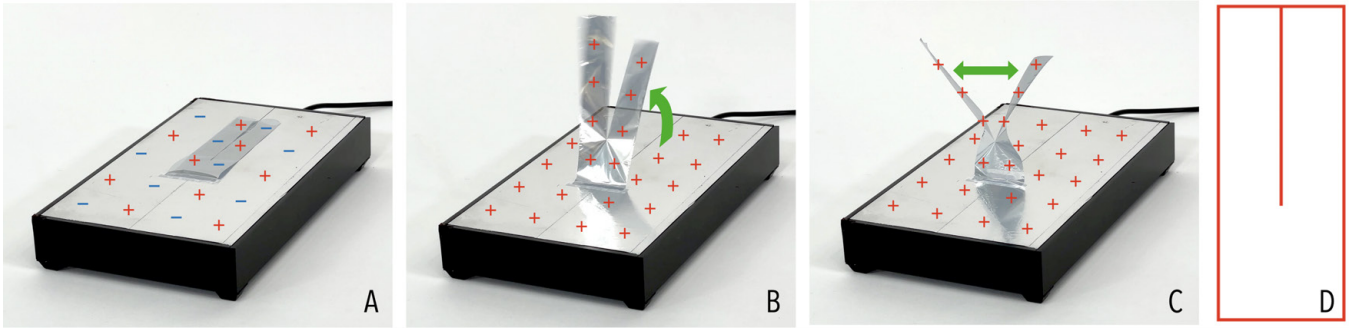

Figure 2: Example mylar sheet with a small cut, attached to our actuation base (A). Upon application of a static charge, the base and mylar sheet repel (B, green vector), owing to their like charges. Additionally, the cut in the mylar sheet causes the two "arms" to repel from one another (C, green vector), forming a Y-like shape. The vector design of the mylar is shown in D.

ratio and their ability to be essentially flat-packed and self-actuate without the need for accessory motors, inflatable polymer film structures have been particularly attractive in space flight applications [7, 33, 52]. In aerospace engineering, they are also known as Gossamer structures or Electrostatically Inflated Membrane Structures (EIMS). Besides applications in aerospace, electrostatic potential and aggregation has been studied in macromolecule-ligand interactions [63] and nanoparticles [28].

We build on this existing literature and consider its utility in the field of human-computer interaction, and shape-changing displays more specifically. We also contribute a new design language and computation tool to help non-expert designers prototype in this new modality. We discuss how forms can be fabricated and used to create new interactive experiences. Finally, we open source our designs and tools to help others replicate and extend this approach.

4 DESIGN AND FABRICATION WORKFLOW

We now describe the materials and tools we employed to design and fabricate our ElectriPop mylar forms, which includes custom hardware and software. We used this workflow to create a series of illustrative outputs targeting application areas of interest.

4.1 Metalized PET

Metalized polyester (PET) film, often referred to as "mylar" (we use this shorthand throughout the paper), has two critical properties that enable our use case. Specifically, mylar is very thin and thus lightweight. This allows the relatively weak electrostatic force (compared to e.g., gravity) to push the structure into new geometric configurations. We found that mylar thicker than 15 microns is too heavy to overcome gravity, lift off its host surface, and fully inflate. Moreover, the thicker the mylar, the lower its elasticity (i.e., its ability to bend), impacting areas that must hinge or twist in order to assume a complex shape. The result is no or partial inflation. The second key property of mylar is its metalization, most commonly a vacuum-deposited layer of aluminum (~0.5 micron in thickness). Although thin, this conductive layer (sheet resistivity of ~10 Ω/square) allows for instant and uniform distribution of static charge across the entire form (as opposed to an insulator, which may only develop a localized charge at the point of contact). For this reason, non-metalized PET will not work for our application.

Mylar can be purchased as bulk rolls and spools for industrial purposes, as well as in a wide variety of consumer goods, including emergency blankets, balloons, and decorative foils. We mostly used 2.4 micron mylar cut from a spool, which we found to be an excellent balance between durability, elasticity and weight. We occasionally used consumer products (art foil is ~15 micron in thickness) as a way to introduce color to some of our example applications. Manufacturers can produce mylar at almost any size, thickness, color or pattern for a high-volume customer.

4.2 Physical Fabrication

Mylar is renowned for its high strength-to-weight ratio [39], allowing sheets to be very thin (1-350 micron are common) and yet still able to be handled by hand without tearing. Mylar is also non-toxic to handle, and while fumes should always be avoided, the material safety datasheet notes that vapor inhalation and material ingestion are not hazards [48]. These excellent properties mean that a wide variety of cutting processes are applicable. Starting with the most basic, mylar can be cut with hand tools, such as exacto-knives and scissors. We often used such tools to cut down larger sheets into more convenient sizes, but we also occasionally cut entire forms by hand. We primarily used CNC tools able to cut digital vector files, such as hobby-grade vinyl cutters and laser cutters. We also found that we could join two sheets of mylar with a heat sealing machine, though it is far easier to purchase sheets of the appropriate size for your design. If a design needs to be mass produced, commercial processes such as die cutting could be used, which have output rates in the thousands-per-minute.

There are three fabrication complexities with mylar that must be considered. First is that mylar is very lightweight, and for this reason, we always taped our mylar sheets to a back board before laser cutting. Second, processes with heat (such as a laser cutting or heat sealing), will cause the polyester to shrink if not held in tension (the tape we used to affix mylar sheets had the added benefit of solving this problem). Finally, if not handled with care, mylar will accumulate "crinkles" and other blemishes owing to its thinness, though this is purely an aesthetic consideration.

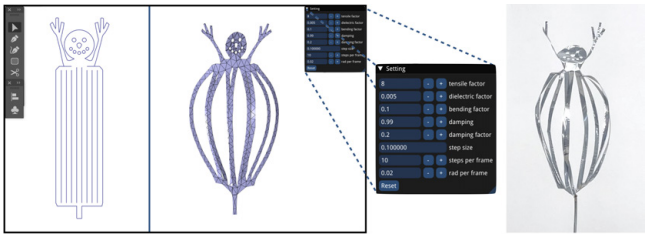

Figure 3: User interface of the ElectriPop design tool. Users use a SVG editing tool (left: Adobe Illustrator CC) to edit the cut pattern in an iterative fashion. A simulator shows the sheet transformation based on the cut pattern in real time. Users can tune the material properties, actuation voltage and simulation parameters on the panel (middle). Right: actual output of an inflated snowman.

4.3 Vector File Design

As we will discuss at length in Section 7, there are a series of design primitives that one can use (and combine) to create complex 3D forms. Fundamentally, this involves making a series of purposeful cuts into a flat sheet of mylar, and thus conventional 2D vector graphics editing programs can be used for design. We created all of our designs in Adobe Illustrator. While graphics programs like Adobe Illustrator are mature and powerful, they do not permit iterative "what you see is what you get" (WYSIWYG) design of our 3D forms. Indeed, the transformation from 2D sheet to 3D inflated object is not always intuitive, and there can also be unforeseen interactions between repelling elements. For this reason, it was necessary to compliment these conventional 2D editing tools with a custom physical 3D simulation program, described in the next section, allowing users to see their output without having to physically fabricate each output.

5 SIMULATION TOOL

As a compliment to users' favorite vector editing tool, we created a novel simulation tool (Figure 3) that automates the 2D-to-3D transformation. Users can iteratively adjust their design based on the real-time simulation result. A user starts the design by drawing a closed polygonal shape that the user will use as the outline of the mylar design. Once the outline is determined, the user can add cuts within the outline by drawing curves. A cutting curve can be either a non-intersected open curve or a closed polygon, which will be interpreted as hollowing out an area from the mylar sheet. Every time the user saves the current edit to their file system, our tool reads the 2D design and automatically starts a real-time simulation, which typically takes a few seconds to converge.

We implemented a position-based dynamics model to simulate the transformation behavior of mylar (Figure 4). To simplify the problem, we consider the mylar sheet as a light thin-shell with high stretch energy, low bending energy and uniformly distributed charge, which resembles origami [47]. We first convert the 2D design from a SVG format into a uniform triangle mesh with Constrained Delaunay Triangulation [49]. The weight and charge of the mylar are distributed on each mesh vertex. The quantity of the weight and charge are proportional to the vertex area. Based on

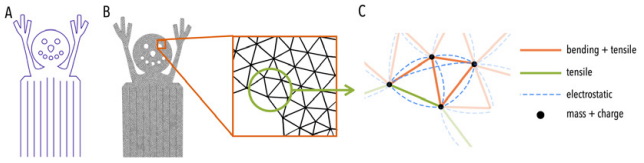

Figure 4: Computation pipeline. The simulator compiles an input SVG (A) into a triangle mesh (B), and optimizes the vertex positions by minimizing the bending, tensile and electrostatic energies (C).

our assumptions, the simulation uses backward Euler as the time integration to minimize the following energies.

Stretch energy — The stretch energy determines how easily the material can be stretched. We add stretch energy on each mesh edge e as $E_t = \frac{EA}{l_0}(l - l_0)^2$, where E is the Young's Modulus, A is the cross-section area of mylar, l and l_0 are the current and original length of e.

Bending energy — For every non-boundary edge, we added bending energy to model the bending stiffness of mylar. Specifically, it prevents the change of dihedral angle of each pair of adjacent triangles. Bending energy $E_b = -k_b \cdot B \cdot l_0(\theta - \theta_0)\frac{\partial\theta}{\partial p}$, where k_b is a constant, B is the bending modulus of the material, θ and θ_0 are the current and original dihedral angle of e, and p is the node positions.

Electrostatic energy — For each pair of vertices in the mesh, we computed the electrostatic energy following Coulomb's Law. Electrostatic force is a long-range force which results in $O(N^2)$ complexity of computation, where N is the number vertices on the mesh. To speed up the simulation and achieve real-time performance, we applied Shifted Force Method [59] to add a continuous cutoff for the computation for electrostatic energy. We remove the cutoff when the model converges to further improve the accuracy without sacrificing efficiency. In addition, we used openMP [10] to parallelize the simulation.

5.0.1 Parameter Search and Optimization. We initialized the mechanical parameters of our model using material specifications of mylar [53]. To further refine these parameters, we ran a parameter search using our simulation tool. More specifically, we physically inflated three designs — compound slits (Figure 8), nested flaps (Figure 11) and dragonfly (Figure 12) — and photographed their 3D forms. In 3D CAD software (Blender), we replicated their 3D shape to serve as a ground truth. While using a 3D scanning tool (e.g., laser scanning, photogrammetry) would have been faster, we did not find any that would robustly capture our thin and reflective mylar forms, and so hand posing was necessary.

We then ran our simulation tool over a grid of possible parameters (see previous section). In pilot tests, we found that mylar had essentially zero stretch (at least at the forces we consider), and so we dropped this from our search. This leaves two main parameters of interest: bending energy and electrostatic energy. For each pair of values, the simulation was run on an input SVG, with output compared to the previously prepared ground truth 3D model. We compare matched pairs of vertices to calculate the mean euclidean error. The results of our grid search can be seen in Figure 5. The

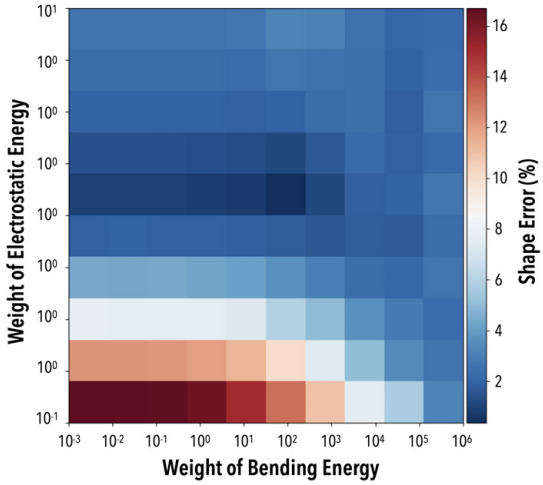

Figure 5: We tuned the parameters of our simulation tool by running a parameter search on bending and electrostatic energies. The darkest blue cell indicates the optimal weights to achieve the best match to real-world output.

simulation found only a slight modification of values was needed achieve an optimal matching between simulated and real-world results (darkest blue cell in the center of the grid; minimum error: 1.03%). We adopted these found parameters for all subsequent studies.

6 ACTUATION HARDWARE

Actuating our mylar forms requires two forces working in tandem. First, we need the mylar to repulse from itself (and thereby inflate) by charging it with static electricity. Second, it is also desirable for the object to rise from a base to increase its visibility (which also helps maximize inflation). The latter bottom-repelling force is achieved by having a metal base which also becomes charged – as the base is heavy and sitting on a table, it does not move, and instead the lightweight mylar form pops upward. A single static generator can able to "pop up" many mylar forms at once (e.g., Figure 15), and can also be multiplexed between different bases (e.g., Figure 19).

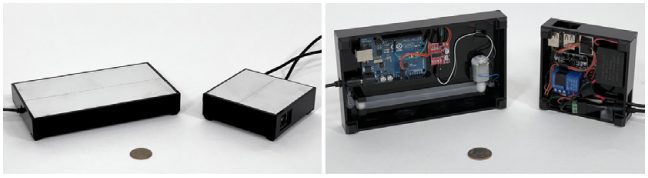

Figure 6: We constructed two, proof-of-concept, digitally-controlled, static generators. Both generators are housed in acrylic boxes with aluminium foil tape on their tops (a). The base on the left is built around a miniature Van der Graaff generator controlled by an Arduino, while the base on the right is solid state and uses a Raspberry Pi (b). A US quarter coin is used for size reference.

As a proof-of-concept, we constructed two bases containing actuation electronics. Both are acrylic boxes with aluminum foil tape applied to the top, seen in Figure 6. One base, measuring $18.2\times 10.8\times 2.8cm$ ($length\times width\times height$), is built around a miniature Van der Graaff generator (using a DC-motor-powered silicon rubber belt running between a PTFE and steel pulley) controlled by an Arduino. Our second base largely follows the design in [16]. It is $10\times10\times3.5cm$ ($length\times width\times height$) in size and uses a low-current 12V to 9kV transformer from a handheld static grass applicator used in building terrain miniatures. The transformer is controlled by an opto-isolated relay connected to a Raspberry Pi, which can connect to the internet and act like an IoT device, allowing the base to display real-time data or be remotely triggered. For both bases, the bill of materials was under $10 USD, not including the Arduino or RaspberryPi, which would be replaced with a lower-cost microcontroller in a real product. Both bases are comparable with minor differences; the motor-powered base is noisier, while the transformer version allows for more dynamic control of voltage.

7 DESIGN SPACE

We now outline a set of design primitives we identified that serve as building blocks for creating interesting 3D forms. While we endeavor to provide explanatory illustrations, many of the 2D-to-3D transformations are hard to visualize. For this reason, we encourage readers to also consult our Video Figure. Better yet, readers are encouraged to download our open-sourced designs (see Section 8), buy an inexpensive static generator[1] and experiment themselves.

7.1 Cuts

We define a cut to be a split made in material that extends to a design's outer edge on one side. This creates two parallel mylar regions, illustrated in Figure 2. Upon application of a static charge, these two regions will attempt to repel. As they are constrained by shared material at one end of the cut, they cannot simply repel outwards to form a flat Y-shape (the tensile strength of mylar is much too great to permit this type of stretch). Instead, the two regions will twist slightly, such that they are no longer in the same plane and will partially face one another. The two faces induce a strong repulsion effect causing the two sides of the cut to push

[1] https://sci-supply.com/fun-fly-stick-ultra-portable-van-de-graaff-generator/

Figure 7: A slit in the film creates two parallel regions which repel to form a loop upon application of electrostatic charge.

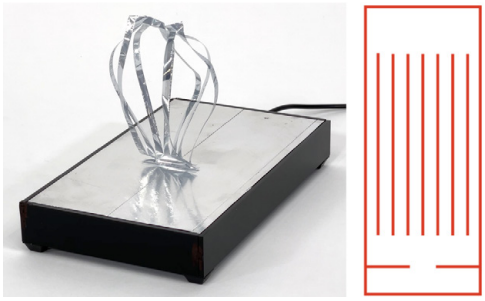

Figure 8: Multiple parallel slit cuts create ribbon-like features which repulse one another to form a sphere-like structure upon application of electrostatic charge.

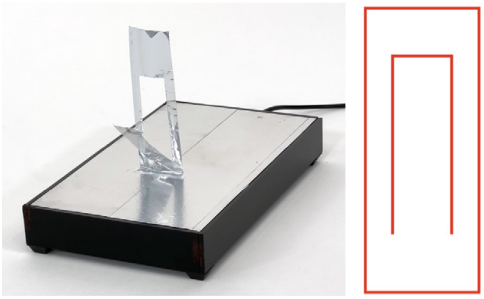

Figure 10: A flap cut encloses an area of mylar which then repulses from the main mylar body, creating a flapped feature hinged on one side.

apart in a non-flat, Y-shape. Cuts can be of any length, though the repulsion effect diminishes with distance from the base, and gravity will cause elements to "droop" if too long or if the repulsion force is too weak.

7.2 Slits

Slits are similar to cuts, but the split in the material terminates inside of the design on both ends. As before, this creates two parallel regions of mylar that repel apart when charged. Just like with cuts, mylar does not stretch at these low forces, and so the two regions deform into an out-of-plane looped shape (as opposed to an in-plane 'O'), seen in Figure 7. The larger the slit, the larger the loop, and the better it approximates a circle. Too small of a slit, and the electrostatic forces are not strong enough to bend the mylar into a loop (more discussion in the Hinges section below). Like cuts, there is no inherent limitation with regards to slit length.

7.3 Compound Slits

As noted above, a single slit forms an O-like shape, which is the building block for creating a sphere. Indeed, by arraying a series of slits in parallel, a series of loops are formed when electrostatically inflated, These ribbon-like features then repulse from one another, fanning out into a sphere-like shape (Figure 8). One can think of this like a sparse wireframe object — the more ribbons, the closer the spacing between ribs in the sphere. Figure 9 shows the result of 4, 6, 8, and 10 slits on the same sized sheet of mylar.

Another important parameter we found was the length-to-width ratio of the ribbons. As noted above with a single slit, bending flat mylar into a curved shape requires force. If the ribbons are too short or too wide, they will not bend enough to assume a 3D shape. With our 2.4 micron mylar, we found a ribbon length-to-width ratio greater than 20:1 had the best results. We also note that deforming from a flat sheet into a sphere means the form's width expands while the height shrinks (a positive Poisson's ratio). This is because ribbons that previously followed (approximately) the diameter of the sphere now follow half the circumference (a ratio of $\frac{\pi}{2}$ in change of height). For the best results, spheres should be cut from sheets with greater height than width — we recommend ratios of 3:1 or greater.

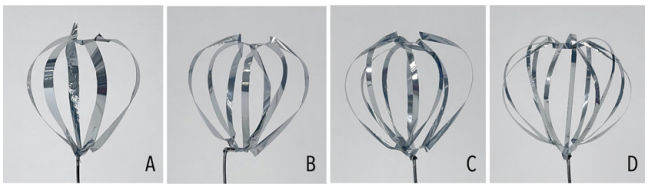

Figure 9: Mylar with compound slits. From left to right: 4, 6, 8, and 10 slits on the same sized sheet of mylar. As the number of slits increases, the increased number of ribbon form a more dense sphere-like shape.

7.4 Flaps

Flaps are a special type of slit, where the cut does not follow a straight line, but rather encloses an area of mylar. When the film is charged with static, the enclosed area repulses from the main mylar body, creating a flapped feature hinged on one side (Figure 10). Most often the surface area of a flap is a smaller feature than than that of the main body, and so the flap is typically deflected proportionally more.

7.5 Nested Flaps

Similar to compound slits, interesting 3D geometries can be created by arraying many cuts together. As noted above, flap features inherently enclose areas of mylar, which can then be augmented with cuts, slits and flaps. One technique we used in several of our designs

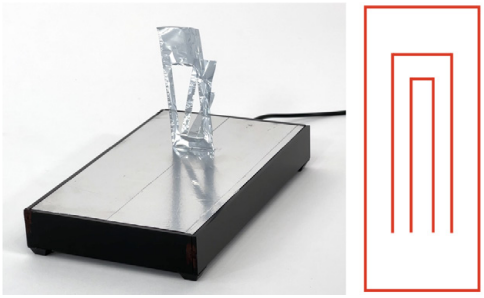

Figure 11: Multiple nested flaps create a repeated geometric elements that repel at different angles.

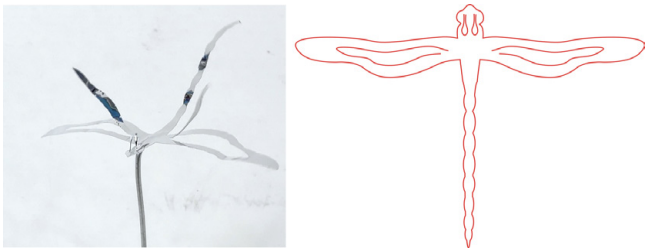

Figure 12: This dragonfly design uses nested flaps to create wings that repel from one another.

was nested flaps (Figure 11). These allowed us to repeat geometric features, such as doubling the wings of a dragonfly (Figure 12) and creating a contoured clamshell (Figure 13). More complex nested flaps are possible, such as the four-sided pyramidal example seen in Figure 14 (and a conical Christmas tree seen in Figure 22). We note that many advanced techniques in Kirigami (a variation of origami that includes cutting) are applicable for our electrostatically inflated mylar objects, and we point interested readers to Chang et al. [6] for an excellent overview of this art form.

7.6 Hinges

When a mylar feature is repelled, the region where it attaches to the main body acts as a "hinge", bending in response to torque from electrostatic repulsion. A simple hinge example can be found at the base of a flapped element, where it hinges like a door (Figure 15). However, this hinging area is also present in less obvious places, such as the ends of slits, where the two sides twist out of plane and also repel (Figure 7). In general, the more material that must hinge, the greater the resistive force, and the less deflection. By adding cuts to the hinge area, we can reduce the amount of mylar that must be bent. As the repelling torque remains the same, the effect is that deflection increases.

7.7 Object Silhouette

An easy and effective way to add character to an object's design is to vary its outer shape. This can be used to create whole-object silhouettes, exemplified by our avatar heads in Figure 16. It can also add flair to smaller elements, such as the thorns on the stem of our flower example (Figure 1) or suckers on our squid's tentacles

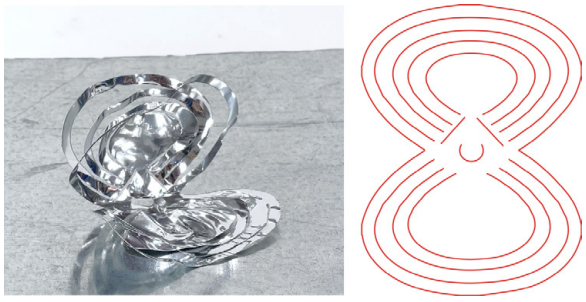

Figure 13: This clam example uses nested flaps to create a contoured shell.

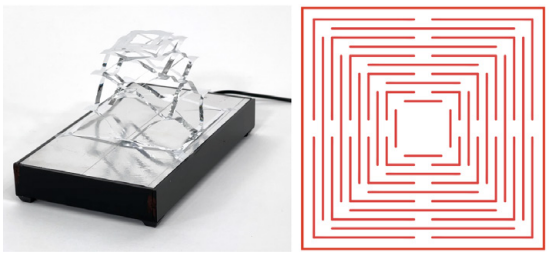

Figure 14: This example of complex nested flaps, a kind of kirigami, forms a pyramidal shape upon inflation.

(Figure 20C). The latter are too small to significantly contribute to 3D form inflation, and thus are purely ornamental.

7.8 Internal Embellishments

Finally, and perhaps most straightforward, designers can add small slits and holes to create negative space interior embellishments that do not strongly participate in object-level 3D inflation. Thus, like silhouettes, they are chiefly ornamental. A good example of internal embellishments are elements like eyes, eyebrows, mouth, hairline, and shirt buttons in our avatar heads (Figures 16 and 17). In our flower example, we added veins to our leaves (Figure 1). We found that well-placed small details help bring designs to life, but unsurprisingly require more artistic talent.

8 OPEN SOURCE CODE AND DESIGN

We are strong proponents of open source fabrication tools for makers, and so we make our simulation tool freely at https://github.com/FIGLAB/MylarFilmSimulator. We additionally provide all of the object examples used in this paper as useful entry points to those wishing to explore this shape changing display modality. Readers can purchase inexpensive, handheld Van der Graaff generators online.

9 EXAMPLE OUTPUT AND USES

To illustrate the creative potential of our technique and workflow, as well as its varied output forms, we created small demos in four application domains: embodied avatars, ambient displays, pop-up books and augmented conventional objects. Please also see our Video Figure.

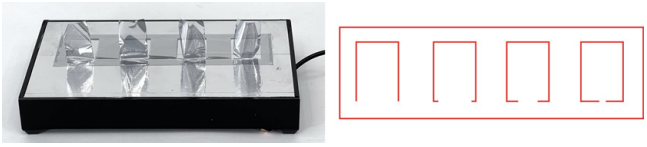

Figure 15: Hinges are created at the end of a flap to allow for more repulsion. The longer the hinge, the easier the cutout can be bent away from the main body during repulsion.

Figure 16: This avatar head uses a combination of a silhouette cut and internal embellishments.

9.1 Embodied Avatars

Smart Speakers have assistive agents that communicate through voice, but do not have physical form beyond the speaker itself. Upon activation, a light ring or other visual indicator is most often used to show the user a listening or active state. As an alternative, we envisioned physical anthropomorphic avatars that can popup from the top of smart speakers upon activation. As a first example, we instrumented an Amazon Echo Dot speaker with a metal foil top and static generator, on top of which we attached a full-body butler design (Figure 17A). Upon activation, the 40cm tall butler avatar springs to life. As a second demo, we similarly instrumented a larger Amazon Echo speaker. Instead of a fixed avatar design, users can personalize their smart speaker agent by choosing among easily-swappable pucks with different head designs (Figure 17B).

9.2 Ambient Displays

Ambient displays [64] are generally designed to convey small quantities of information without demanding a user's full attention. They are often designed as aesthetic objects that reside in a user's environment. Shape-changing technologies are widely used in this space, and we drew on the literature for inspiration. For example, Elliot et al. [11] created a small flower garden that could be actuated. Similarly, we created a mylar flower with a programmatically-controlled wilting level (Figure 18). Such a display could convey information on a loved one's physical activity, stock market performance, water consumption and any other digitally-accessible value. As a second demo, we created a weather ambient display. Three independently

Figure 17: A) We instrumented an Amazon Echo dot with a 40cm pop-up butler, which could activate upon speaking a wake word. B) Users could also personalize their smart speaker agents with inexpensive (<$1) and swap-able avatar pucks, which rest on top of the speaker.

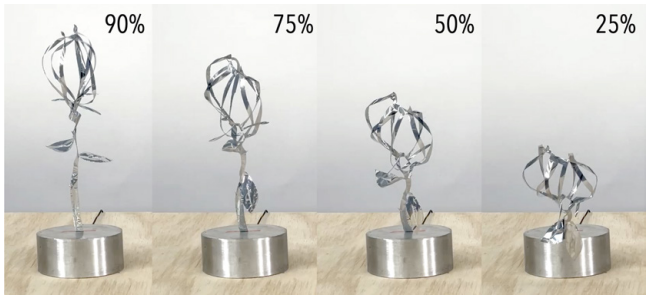

Figure 18: By varying the level of electrostatic charge, we can control the level of inflation. This could be used for more expressive ambient displays, such as this wilting flower.

actuated mylar elements (using three relays connected to a single static generator) — a lightning bolt, cloud, and sun — raise and lower to display the forecast (Figure 19).

9.3 Pop-Up Books & Decorations

The thin, paper-like quality of mylar sheets makes them well-suited for use in popup books, opening new designs not possible with traditional folded paper techniques. As a proof of concept, we instrumented a few pages of a children book with pop-up mylar elements, including seaweed, a squid attacking a fish, and a clam opening (Figure 20, B-D). Sandwiched between pages is a thin aluminum foil layer that distributes the static charge and provides a repelling effect from the surface of the page. Rather than including actuation electronics in the book itself (which at $10 would exceed the cost of the book), we use a handheld static generator that can be reused across books. To activate a page, the user touches the "wand" to a special conductive region at the corner of the page (Figure 20A, closeup).

The flat geometry of our designs also means they can be easily mailed (Figure 22), and their low cost makes them amenable for uses such as pop-up holiday cards and decorations. As one example, we created a popup Christmas tree (Figure 22).

9.4 Augmenting Conventional Objects

As a final example category, we considered how our technique could be used to inexpensively add dynamic animated elements to conventional objects. Although this requires running single-wire conductive pathways to attachment points, this is still far cheaper than most prior actuation approaches (e.g., DC motors, solenoids,

Figure 19: This weather ambient display has three independently controlled panels for lightning, clouds, and sun.

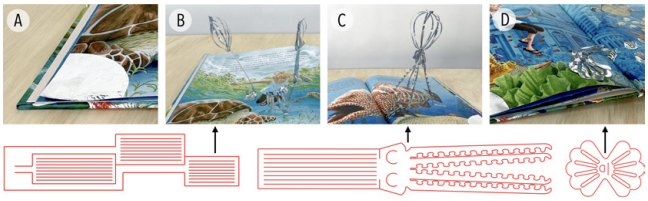

Figure 20: We instrumented a book with popup elements. To activate a page, users touch a handheld static generator to a special region in the corner of each page (A). This inflates features such as seaweed (B), squids (C), and clams (D).

shape memory alloys, pneumatics, fluidics, peltier junctions). As one example, we instrumented a trophy with pulsating steamers emanating from the plaque and wings that twitch on a Quidditch ball (Figure 21).

10 EVALUATION

There are three important aspects of our technique that we wished to study: 1) What are the physical performance metrics that underpin our method, such as inflation time and discharge rate? 2) How closely does our simulation tool match the actual physical output? 3) Can users effectively apply ElectriPop and our design tool to create artifacts? To begin to answer these questions, we ran three investigations, which we now describe.

10.1 Performance Characterization

In order to compare against other shape changing methods, as well as more deeply understand the physics of our technique, it was important to characterize ElectriPop's behavior. For these experiments, we used our transformer base (Figure 6), which has an output voltage of 9kV when powered at 12V.

10.1.1 Electrical Inflation. We measured the time and power required to flood the mylar film with charge (which is different from the time needed to physically inflate, which we describe next). Using our snowman design (Figure 3), we measured the amount

Figure 21: Conventional objects can be inexpensively instrumented with ElectriPop elements, such as the wings and streamers on this Quidditch trophy.

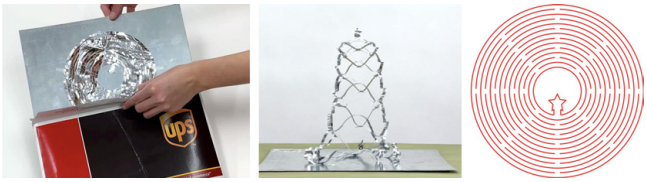

Figure 22: A popup Christmas tree can be mailed flat-packed and then inflated into its volumetric.

of current required to electrically "inflate" our base and snowman design using a floating (non-grounded) multimeter with a known resistance of 9MΩ. The average steady-state current is V/R =11.5V/9MΩ=1.28μA, where V is the measured voltage, R is the resistance of the multimeter. Using a high voltage probe with a resistance of 1GΩ, we also measured the amount of current needed for the voltage converter, which is V/R =6.80kV/1GΩ=6.80μA, where V again is the measured voltage, R is the resistance of the high voltage probe. According to International Electrotechnical Commission's IEC 62368 standard, both current inputs are below the ES1 current limit [1]. In other words, the power source is not capable of supplying dangerous steady-state current, and the system does not require a significant amount of current to be inflated. In terms of duration, it takes on the order of 10 milliseconds to fully saturate the mylar with charge (it acts like a capacitor being charged with a current-limited source).

10.1.2 Physical Inflation. As the mylar charges, it begins to repel and physically inflate. The repulsion force has to overcome gravity and bend mylar, which wishes to stay flat. Air resistance also works to retard physical inflation. On average, our snowman design takes around 100ms to fully inflate, and inflation times were remarkably consistent. In contrast, our largest and heaviest design, the Christmas tree, takes ~750ms to inflate.

10.1.3 Electrical Deflation. We also measured how our mylar forms electrically deflate when grounded. For this, we used a 1kΩ shunt resistor to simulate the resistance of a finger. We used an oscilloscope probe attached to the resistor and recorded the voltage across the resistor to measure the discharge current (Figure 23, blue line) when the resistor contacts the system (in this case, an inflated snowman design), and we integrated the current to get the initial charge of the system (Figure 23, green line). The total discharge is 16.3nC. The time constant τ, which is the time it takes to reach 63% of steady-state is 39.5ns (Figure 23 red dash line). Since $\tau = R \times C$, where R and C are the resistance and capacitance of the system respectively, we can derive the capacitance of the system, which is 39.5pF. This is an insignificant amount of charge and the system's capacitance is extremely small compared to the IEC 62368 standard [1]. As discharge is not current limited (unlike inflation), electrical discharge times are very fast — 160ns on average. This also allowed us to estimate the initial voltage before discharge V=412V using $V = Q/C$, and the stored energy before discharge E =6.68μJ, using $E = 0.5 \times Q \times V$, where Q in both equations is the total discharge.

There is also natural electrical deflation over time due to e.g., water molecules in air slowly bleeding charge. The rate of discharge depends on factors such as object surface area, ambient humidity

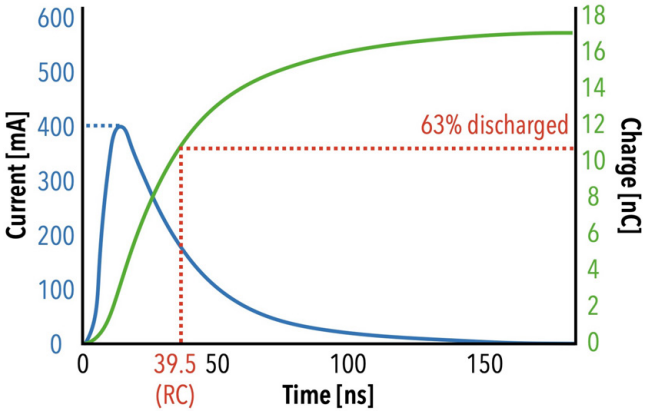

Figure 23: We recorded the forced discharge current output over time (blue line) of an inflated snowman design and then integrated the recorded value (green line). We used 63% of the steady-state value to calculate the system's capacitance.

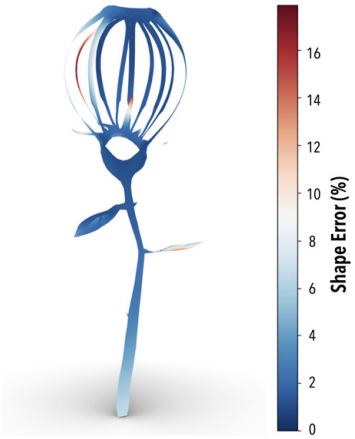

Figure 24: Distribution of the Euclidean error of a simulated flower design compared to its actual 3D output.

and airflow. However, in general, the discharge rate is low and was not a significant hindrance in our designs. For example, without periodic recharging, our flower deflates in 25 minutes (at 22.3 °C, 19% relative humidity). Thus, to keep forms fully inflated, we suggest momentary charge boosts every five minutes or so.

10.1.4 Physical Deflation. Our snowman example takes 67ms to physically fall once static electricity is discharged and the repulsion force becomes absent. Note that this is faster than inflation, as deflation is assisted by gravity and stored spring forces that want to pull the mylar back to its original flat form. Working against deflation is air resistance, the magnitude of which is highly dependent on object geometry (i.e., in some designs, the form can act like a parachute, slowing deflation).

10.1.5 Volumetric change. Using our simulation tool, we characterized the volume of our snowman cutout (2.5 microns thin with a surface area of 19.20cm^2) and its total volume after inflation (104.49 cm^3). Thus the total percentage increase in volume is roughly 200,000%.

10.1.6 Fabrication Time. As noted earlier, our designs can be cut by many different technologies that range from slow and laborious (e.g., scissors — one output after several minutes) to fast and precise (e.g., die cutting — many outputs per second). Laser cutting lies somewhere in the middle in terms of speed, and it is also a tool available in many fabrication spaces. In the case of our snowman example, the cut time is 30 seconds on our ULS 30W CO2 laser cutter (100% speed, 5% power).

10.2 Simulated vs. Real-World Output Geometric Accuracy

To measure the geometric accuracy of our simulation, we compared the 3D model of our simulated result with its real-world output. As noted in section 5.0.1, it was not possible to use a 3D scanning tool (e.g., laser scanning, photogrammetry) to automatically create a 3D model of our physical output, due to the thin and reflective nature of mylar. Instead, we manually created a 3D model that matched the physical output, creating a ground truth. We did this for our rose, snowman, and Christmas tree designs (Figure 1B, 3, 22 respectively). Now, with both a 3D model of the physical output and a 3D model of the simulated output, we can iterate through all vertices to compute the distance error between the two models. To remove rotation as a factor, the base vertices in both models are aligned. We ran our simulations 100 times on a computer with an X3900 RYZEN CPU. Table 1 also reports the average simulation convergence time for each design. Simulation for most designs takes around ten seconds to fully converge, and the user is able to watch the simulation play out in real time.

Across all simulation trials, we found a mean 3D euclidean error of 1.55mm. Broken out by design, our rose, Christmas tree and snowman simulation results had errors of 3.43mm (SD=0.34), 0.75mm (SD=1.30), and 0.46mm (SD=0.15) respectively (Table 1). Qualitatively, we found that the models largely matched in gestalt. While there were small variations, often accessory details, these were more often than not "correct" answers, and the output depended on how the form was inflated or perturbed from airflow. Put simply: the simulated result was not incorrect, but rather a different correct state. This can be seen in Figure 24, which visualizes the error distribution for our worst performing output: the flower. Note that most of the form is in dark blue (accurate), with a few errorful regions (shades of red) that are still plausibly posed. Overall, our empirical results match our observations that our simulation tool could be relied upon to provide a preview of the 3D form.

Design	Triangle Count	Steps / Second	Steps to Convergence	Time to Convergence [s]	3D Euclidean Error (SD) [mm]
Rose	289	213.9	1780	8.3	3.43 (0.34)
Snowman	322	225.4	2000	8.9	0.46 (0.15)
Christmas Tree	1040	58.3	10150	174.0	0.75 (1.30)

Table 1: Simulation performance of example designs.

Actuation Method	Electrostatic Repulsion	Manual	Pneumatic	Microfluidic	Electro-hydraulic / Dielectric Elastomer	Electric Phase Change	Electro-mechanical	Thermo-reactive	Moisture-reactive
Reference Systems	ElectriPop	Pop-up Books	MorphIO [41], LiftTiles [54], PneUI [65]	milliMorph [34]	Franinović and. Franzke [15], ElectriFlow [42]	Nakahara et al. [40]	inFORM [13], ShapeShift [51]	Thermorph [4], NURBSforms [55], Printed Paper Actuator [61]	bioLogic [66], Transformative Appetite [62]
Material	Metalized mylar	Paper	Silicone, plastic, paper	PET, liquid, conductive ink	PET, dielectric fluid / acrylic elastomer, silicone, carbon black	Thermoplastic, PET, low boiling point liquid	Pin array, DC motors	Thermoplastics, shape memory alloy, paper	Organic material
Fabrication Method	Laser cutting	Folding, cutting	Heat sealing, silicone molding	Sealing, injection	Heat sealing, liquid filling, cutting / stretching, coating	inkjet printing, plotting, heat sealing	Mechanical assemly	3D printing, etching, laminating, soldering	Inkjet/CNC printing
Fabrication Time	<1 min	–	~30 min	Not reported	Not reported	30 min	Not reported	60 – 90 min	Not reported
Actuation Time	0.1 – 0.75 sec	<1 sec	1.1 – 16 sec	2 sec	~0.05 sec	35 – 90 sec	0.64 – 0.75 m/s	4 – 15 sec	15 sec – 2 min
Reversal Time	0.07 sec	<1 sec	1.1 – 4 sec	5 – 7 sec	~0.05 sec	10 – 15 sec	0.81 – 0.97 m/s	7 – 20 sec	15 sec
Idle Thickness	0.0025 – 0.012 mm	0.2 mm	~150 mm	0.040 mm	0.025 – 6 mm	0.12 mm	–	0.2 – 1.2 mm	0.0036 – 0.08 mm
Volumetric Expansion	200,000 – 300,000%	–	~1000%	low (curvature 0.35 mm^{-1})	low (bending angle ~50°)	low (bending angle ~90°)	9 – 32%	27% / bending angle 110° – 200°	low (curvature ~0.25 mm^{-1})
Power Consumption	0.068 W	n/a	1.13 – 73 W	Not reported	~ 1 W	3 – 15 W	300 W	~1.52 W	Not reported
Noise Level	Silent	Silent	55 – 72 dB	Silent	Not reported	Not reported	Modest	Silent	Silent

Table 2: Comparison of ElectriPop with other shape-changing methods.

10.3 User Experience Investigation

To study our design process and simulation tool, we recruited eight participants (mean age 24). All had prior experience using a vector editing tool, and half were designers with at least some familiarity of computational design principles. The design session lasted roughly one hour and paid $20 in compensation.

We first explained to participants the workflow and operating principle of ElectriPop. We then showed participants example design primitives and invited them to run the simulation tool on a couple of these designs to familiarize themselves with the tool and process. We then asked them to prototype a three-dimensional design of their choosing with a time budget of 30 minutes. Following this design session, participants filled out a four-question survey on a seven-point scale (1 — strongly disagree, 7 — strongly agree): Q1: I was able to come up with a design using the library of primitives. Q2: I was able to iteratively improve my design using the simulation tool. Q3: I was able to achieve the 3D output I had in mind with the system. Q4: I am interested in using this technique in my future creative projects. The design session concluded with a semi-structured interview.

Overall, the participants were able to utilize the provided tool and design exemplars to create their own designs (Q1: M=6.25, SD=1.04). They found the library of primitives "easy to understand" (P3) and "help[ed] explain the technique" (P6). They were also able to iterate on their design using the simulation tool (Q2: M=5.50, SD=2.00) and found the experience "seamless" (P5) and "help[ed] them build intuition of the [method]" (P8). Participants appreciated that they could see the simulation results in real-time and felt the tool saved them time during the iteration process. Participants created a variety of designs, some were more geometric while others resembled real-life objects. While most participants were able to create the designs they had in mind (Q3: M=4.88, SD=1.73), some expressed that the initial step of creating a 2D design of a 3D form was difficult. Thus, the ability to directly modify the 3D output through an inverse design tool would likely be a significant boon. Lastly, participants found the technique to be interesting (Q4: M=5.75, SD=1.58) and could be used to create interactive installations and ambient devices. Some participants commented on other ways they would attempt to achieve similar actuate-able 3D output, which included gluing together layers of film and use a fan to blow air on the structure, or 3D print a mechanism, which they noted would be a significant amount of design work.

11 COMPARISON TO OTHER SHAPE-CHANGING METHODS

Table 2 provides a high-level comparison of ElectriPop to representative examples of other shape-changing methods across a range of important criteria.

Among the shape-changing techniques, ElectriPop's use of electrostatic force as the actuation method is unique, opening new forms and capabilities in shape-changing output. Typically, to achieve a complex 3D form, multiple layers and materials are involved to achieve the desired structures and transformations. ElectriPop's use of a single layer of bulk material permits easy and quick fabrication relative to other methods, while still offering creative outputs. Mylar can also be cut at a very high speeds and even mass produced (e.g., die cutting), which makes fabrication efficient compared to e.g., multi-material 3D printing.

We also note that our technique does not use pumps or sealed bladders like most inflatable systems, which are more complex to manufacture and maintain (i.e., keep air- or liquid-tight). Further, ElectriPop forms do not require any integrated motors or exoskeletal structures, allowing the mylar to be completely flat-packed, and thus highly transportable and lightweight. Compared to most other methods, such as thermo- and moisture-responsive materials, ElectriPop's shape-changing effect is near instantaneous. Once inflated, our forms can hold their state for long periods of time, which is energy efficient. Our forms can also revert back to their pre-inflated

state quickly, and can be toggled on/off rapidly (or even held at intermediate charge states). Unlike most motor- and pump-based systems, our technique is essentially silent in operation (particularly our solid-state transformer-based implementation). It is also very energy efficient (tens of mW) and can be battery powered.

This combination of desirable properties — fast transition speeds, low-cost, easy-fabrication, energy efficient, and quiet — makes ElectriPop an interesting addition to the shape-changing interface literature. Of course, like all methods, ElectriPop has downsides and limitations, which we discuss next.

12 DISCUSSION AND LIMITATIONS

Over the course of our explorations, we had many smaller findings and insights, including limitations, which we briefly summarize.

Computational Tool – Our proof-of-concept simulation tool runs interactively for meshes comprised of upwards of 1000 vertices. For many designs, this is sufficient geometric resolution. Nonetheless, there are avenues to increase performance, such as moving to Particle Mesh Eward methods [25] or MSM methods [35]. We also note that although our simulation tool helps to speed up the design iteration process (and saves fabrication time and cost), the overall design process is still very much trial-and-error. A semi-inverse design tool [45], where a user could directly modify the desired 3D form (with the computer generating the 2D cut pattern), would be valuable to explore in future work.

Size & Volume Limitations – We found it was difficult, if not impossible, to actuate mylar structures greater than 40cm in height. As the electrostatic force needs to overcome the "compressive" 1G gravitational force, the heavier the material or the larger the cutout, the bigger the force it needs to overcome. Higher voltage or larger repelling bases could extend range, but at the cost of practicality. Alternatively, by changing the geometry of the cutout – making the individual ribbons thin and elongated as well as adding hinges (as we described in Section 7.3 and 7.6) – can compensate for large and/or heavy material.

Geometric Limitations – Although our system demonstrates promise in creating complex, volumetric shapes, there are some geometries we did not achieve, such as a cube or cylinder. These forms might be possible, drawing on techniques used in practices such as kirigami. We also note that we limited our explorations to making cuts in a single, flat piece of continuous material, but multi-layered forms with structured joins could no doubt achieve even more complex geometries; an area we leave to future work. We did briefly experiment with a plastic sealing machine, which can successfully join two pieces of mylar together (glues can also be used).

Actuation Speed – The transformation of the mylar cutout from 2D to 3D is very fast. Please see Section 10.1.1 for an extended discussion on this subject. Briefly here: our snowman example takes ~100ms to be fully inflated, whereas the larger Christmas tree takes ~750ms. Overall, our technique's actuation speed compares favorably to other actuation methods (pneumatics, fluidics, shape-memory alloys).

Multiplexing – As we demonstrated in our ambient weather display (Figure 19), it is possible to independently control different elements. These are simply independent displays arrayed together, with relays that ether connect them to a static source (to inflate) or to ground (to deflate).

Static Charge Safety – Human naturally accumulate electrostatic charge as we go about our daily lives [27], from sitting in a chair, taking off clothing, walking across a floor, and opening a package. Most often it is unnoticed, or perhaps an minor annoyance (e.g., packing peanuts that stick to your body). However, at higher voltages, one feels a momentary sting at the moment of electrostatic discharge (ESD). Research has found that walking across a carpet can generate 15kV [27, 29], while making a bed can go as high as 38kV [31]. Our operating voltages are around 10-15kV, and while unpleasant to touch, are safe. As mentioned in Sections 10.1.1 and 10.1.3, both the current draw and capacitance are significantly below international standard's limits. As humans naturally accumulate static charge, most consumer devices are built to tolerate some level of ESD. Nonetheless, our use of static charge makes touch interaction less desirable (plus the fact the form discharges and deflates immediately upon contact). To entirely remove the possibility of touching a charged form, bases could include a commodity proximity sensor (e.g., infrared, ultrasonic) that detects if a user or object is too close (e.g., less than 1 m), and immediately discharge the form.

User Interaction — As mentioned in the section above, we do not encourage users to make contact with mylar structures when electrostatically charged. However, we do note there is an interesting effect wherein the mylar leans towards the user's hand or body when proximate (Figure 25 and Video Figure). This imbues a lifelike

Figure 25: Users' hand create an electrostatic attraction with inflated designs, which lean toward the user.

Figure 26: An avatar attempts to get the user's attention by flailing its arms.

quality to otherwise passive forms, offering a sense of attention and interactivity. This effect can be seen in our Video Figure at 2:18.

Animation — We found that we could create primitive animations by varying the level of voltage, creating waves of repulsion that cause features to undulate. As one example, we created a butler avatar that can wave its arms to get the user's attention (see Figure 26 and Video Figure). As a more subtle example, we also animated our clam (Figure 20D) to slowly open and close.

Form Collapse & Tangling — When a discharge happens, the mylar becomes neutral and falls per gravity and air resistance. In the process of free-falling, the mylar film collapses with some variability. In some cases, the film could fall outside of the perimeter of its base. We found that to ensure a successful re-inflation after a collapse, the metallic base onto which the mylar film is attached needs to be large enough to "catch" the mylar form no matter which direction it falls. In some instances, free-falling can lead to a tangle in the mylar, which prevents successful full re-inflation. We found the best way to guard against this issue was in the design of a form's geometry.

Colors & Patterns — Mylar comes in an incredible array of colors and printed patterns, often sold as "art foil". If these are thin and light enough (<15 microns), they can be used. We built two of our demos using such materials: gold foil for our trophy (Figure 21) and patterned foil for our ambient weather display (Figure 19).

Durability — The thinness of metalized mylar that makes it easy to electrostatically inflate also makes it fragile, subject to tears and wrinkles. After the mylar is cut, one needs to carefully separate the cutout from the rest of the material and carefully place it on the electrostatic generator base.

Air Flow — Metalized mylar has a high surface area to mass ratio, and thus it is easily disturbed by air flow, whether that be from HVAC or a user walking by. In our experiences, this is never enough to collapse the form, but can cause deflection or twisting of the form. Wider bases can be used to mitigate this effect, or it can be embraced to great effect. For example, it makes our butler avatar shift direction, and feel more dynamic and even alive (see 2:38 in Video Figure). Similarly, air flow causes our rose to twist (2:02 in Video Figure), helping to show off its delicate 3D form.

Humidity — The effect of humidity on electrostatic charge has been extensively researched, as it is of critical importance in many sectors, including manufacturing and health [12, 31]. When humidity is high, the conductivity of air increases, which increases the ambient discharge rate [56]. Thus, in high-humidity environments, more charge is needed to actuate our displays, which must also be periodically refreshed more often.

13 CONCLUSION

We have introduced a new shape-changing volumetric display approach where 2D, flat-packed mylar sheets can be inflated into complex 3D structures using electrostatic force. By placing and nesting cuts, slits, and holes, mylar cutouts can be inflated into various 3D forms via electrostatic inflation. We introduce a design vocabulary to describe these primitives and developed a computational tool to simulate the 3D output to facilitate rapid prototyping. Our system is comparatively low-cost and can be easily fabricated using a variety of methods. We created two compact, proof-of-concept electrostatic generators for actuation, which are fast-acting and nearly silent. We created a series of demos, such as ambient displays and educational pop-up books, to illustrate the applications of our approach. We hope this work inspires new and creative shape-changing interfaces.

ACKNOWLEDGMENTS

The authors thank Dr. Craig Shultz for his guidance on the technical evaluation of this project. This research was partially supported by the National Science Foundation grant IIS-2047912 and the Alfred P. Sloan Foundation.

REFERENCES

[1] International Electrotechnical Commission. IEC 62368-1:2018. [n.d.]. https://webstore.iec.ch/publication/27412

[2] Hillel Aharoni, Yu Xia, Xinyue Zhang, Randall D Kamien, and Shu Yang. 2018. Universal inverse design of surfaces with thin nematic elastomer sheets. *Proceedings of the National Academy of Sciences* 115, 28 (2018), 7206–7211.

[3] Jason Alexander, Anne Roudaut, Jürgen Steimle, Kasper Hornbæk, Miguel Bruns Alonso, Sean Follmer, and Timothy Merritt. 2018. Grand challenges in shape-changing interface research. In *Proceedings of the 2018 CHI conference on human factors in computing systems*. 1–14.

[4] Byoungkwon An, Ye Tao, Jianzhe Gu, Tingyu Cheng, Xiang'Anthony' Chen, Xiaoxiao Zhang, Wei Zhao, Youngwook Do, Shigeo Takahashi, Hsiang-Yun Wu, et al. 2018. Thermorph: Democratizing 4D printing of self-folding materials and interfaces. In *Proceedings of the 2018 CHI conference on human factors in computing systems*. 1–12.

[5] Hrvoje Benko, Christian Holz, Mike Sinclair, and Eyal Ofek. 2016. NormalTouch and TextureTouch: High-Fidelity 3D Haptic Shape Rendering on Handheld Virtual Reality Controllers. In *Proceedings of the 29th Annual Symposium on User Interface Software and Technology* (Tokyo, Japan) *(UIST '16)*. Association for Computing Machinery, New York, NY, USA, 717–728. https://doi.org/10.1145/2984511.2984526

[6] Zekun Chang, Tung D Ta, Koya Narumi, Heeju Kim, Fuminori Okuya, Dongchi Li, Kunihiro Kato, Jie Qi, Yoshinobu Miyamoto, Kazuya Saito, et al. 2020. Kirigami Haptic Swatches: Design Methods for Cut-and-Fold Haptic Feedback Mechanisms. In *Proceedings of the 2020 CHI Conference on Human Factors in Computing Systems*. 1–12.

[7] AB Chmielewski and CHM Jenkins. 2005. Gossamer spacecraft. *WIT Transactions on State-of-the-art in Science and Engineering* 20 (2005).

[8] Gary PT Choi, Levi H Dudte, and L Mahadevan. 2019. Programming shape using kirigami tessellations. *Nature materials* 18, 9 (2019), 999–1004.

[9] Marcelo Coelho and Pattie Maes. 2009. Shutters: a permeable surface for environmental control and communication. In *Proceedings of the 3rd International Conference on Tangible and Embedded Interaction*. 13–18.

[10] Leonardo Dagum and Ramesh Menon. 1998. OpenMP: an industry standard API for shared-memory programming. *IEEE computational science and engineering* 5, 1 (1998), 46–55.

[11] Kathryn Elliot, Mark Watson, Carman Neustaedter, and Saul Greenberg. 2007. Location-Dependent Information Appliances for the Home. In *Proceedings of Graphics Interface 2007* (Montreal, Canada) *(GI '07)*. Association for Computing Machinery, New York, NY, USA, 151–158. https://doi.org/10.1145/1268517.1268543

[12] Incorporated EOS/ESD Association. 2008. *ESD TR20. 20-2008 Handbook for the Development of an Electrostatic Discharge Control Program for the Protection of Electronic Parts, Assemblies and Equipment*. EOS/ESD Association, Incorporated. https://books.google.com/books?id=HIWvPAAACAAJ

[13] Sean Follmer, Daniel Leithinger, Alex Olwal, Akimitsu Hogge, and Hiroshi Ishii. 2013. inFORM: dynamic physical affordances and constraints through shape and object actuation.. In *Uist*, Vol. 13. 2501988–2502032.

[14] Jack Forman, Taylor Tabb, Youngwook Do, Meng-Han Yeh, Adrian Galvin, and Lining Yao. 2019. ModiFiber: Two-Way Morphing Soft Thread Actuators for Tangible Interaction. In *Proceedings of the 2019 CHI Conference on Human Factors in Computing Systems*. 1–11.

[15] Karmen Franinović and Luke Franzke. 2019. Shape Changing Surfaces and Structures: Design Tools and Methods for Electroactive Polymers. In *Proceedings of the 2019 CHI Conference on Human Factors in Computing Systems*. 1–12.

[16] Juri Fujii, Satoshi Nakamaru, and Yasuaki Kakehi. 2021. LayerPump: Rapid Prototyping of Functional 3D Objects with Built-in Electrohydrodynamics Pumps Based on Layered Plates. In *Proceedings of the Fifteenth International Conference on Tangible, Embedded, and Embodied Interaction*. 1–7.

[17] Qi Ge, H Jerry Qi, and Martin L Dunn. 2013. Active materials by four-dimension printing. *Applied Physics Letters* 103, 13 (2013), 131901.

[18] A Sydney Gladman, Elisabetta A Matsumoto, Ralph G Nuzzo, Lakshminarayanan Mahadevan, and Jennifer A Lewis. 2016. Biomimetic 4D printing. *Nature materials* 15, 4 (2016), 413–418.

[19] Jens Emil Grønbæk, Majken Kirkegaard Rasmussen, Kim Halskov, and Marianne Graves Petersen. 2020. *KirigamiTable: Designing for Proxemic Transitions with a Shape-Changing Tabletop.* Association for Computing Machinery, New York, NY, USA, 1–15. https://doi.org/10.1145/3313831.3376834

[20] Jianzhe Gu, Vidya Narayanan, Guanyun Wang, Danli Luo, Harshika Jain, Kexin Lu, Fang Qin, Sijia Wang, James McCann, and Lining Yao. 2020. Inverse Design Tool for Asymmetrical Self-Rising Surfaces with Color Texture. In *Symposium on Computational Fabrication*. 1–12.

[21] Ruslan Guseinov, Eder Miguel, and Bernd Bickel. 2017. CurveUps: Shaping objects from flat plates with tension-actuated curvature. *ACM Transactions on Graphics (TOG)* 36, 4 (2017), 1–12.

[22] David Halliday, Robert Resnick, and Jearl Walker. 2013. *Fundamentals of physics*. John Wiley & Sons.

[23] Chris Harrison and Scott E. Hudson. 2009. Providing Dynamically Changeable Physical Buttons on a Visual Display. In *Proceedings of the SIGCHI Conference on Human Factors in Computing Systems* (Boston, MA, USA) *(CHI '09)*. Association for Computing Machinery, New York, NY, USA, 299–308. https://doi.org/10.1145/1518701.1518749

[24] Felix Heibeck, Basheer Tome, Clark Della Silva, and Hiroshi Ishii. 2015. uniMorph: Fabricating thin film composites for shape-changing interfaces. In *Proceedings of the 28th Annual ACM Symposium on User Interface Software & Technology*. 233–242.

[25] Henry David Herce, Angel Enrique Garcia, and Thomas Darden. 2007. The electrostatic surface term:(I) periodic systems. *The Journal of chemical physics* 126, 12 (2007), 124106.

[26] Lishuai Jin, Antonio Elia Forte, Bolei Deng, Ahmad Rafsanjani, and Katia Bertoldi. 2020. Kirigami-Inspired Inflatables with Programmable Shapes. *Advanced Materials* 32, 33 (2020), 2001863.

[27] Niels Jonassen. 2002. *Static Electricity and People*. Springer US, Boston, MA, 145–150. https://doi.org/10.1007/978-1-4615-1073-4_9

[28] Alexander M Kalsin, Anatoliy O Pinchuk, Stoyan K Smoukov, Maciej Paszewski, George C Schatz, and Bartosz A Grzybowski. 2006. Electrostatic Aggregation and Formation of Core- Shell Suprastructures in Binary Mixtures of Charged Metal Nanoparticles. *Nano letters* 6, 9 (2006), 1896–1903.

[29] MA Kelly, GE Servais, and TV Pfaffenbach. 1993. An investigation of human body electrostatic discharge. In *INTERNATIONAL SYMPOSIUM FOR TESTING AND FAILURE ANALYSIS*. AMERICAN TECHNICAL PUBLISHERS LTD, 167–167.

[30] Yoonho Kim, Hyunwoo Yuk, Ruike Zhao, Shawn A Chester, and Xuanhe Zhao. 2018. Printing ferromagnetic domains for untethered fast-transforming soft materials. *Nature* 558, 7709 (2018), 274–279.

[31] Mehdi Kohani, David Pommerenke, Lane Kinslow, Aniket Bhandare, Li Guan, Jianchi Zhou, Christopher Spencer, and Michael G Pecht. 2019. Electrostatic Charging of a Human Body Caused by Activities and Material Combinations in Hospitals. *IEEE Transactions on Electromagnetic Compatibility* 62, 2 (2019), 315–323.

[32] Mina Konaković-Luković, Julian Panetta, Keenan Crane, and Mark Pauly. 2018. Rapid deployment of curved surfaces via programmable auxetics. *ACM Transactions on Graphics (TOG)* 37, 4 (2018), 1–13.

[33] Zhi-Quan Liu, Hui Qiu, Xiao Li, and Shu-Li Yang. 2017. Review of large spacecraft deployable membrane antenna structures. *Chinese Journal of Mechanical Engineering* 30, 6 (2017), 1447–1459.

[34] Qiuyu Lu, Jifei Ou, João Wilbert, André Haben, Haipeng Mi, and Hiroshi Ishii. 2019. milliMorph–Fluid-Driven Thin Film Shape-Change Materials for Interaction Design. In *Proceedings of the 32nd Annual ACM Symposium on User Interface Software and Technology*. 663–672.

[35] Jordan Maxwell, Kieran Wilson, Joseph Hughes, and Hanspeter Schaub. 2020. Multisphere Method for Flexible Conducting Space Objects: Modeling and Experiments. *Journal of Spacecraft and Rockets* 57, 2 (2020), 225–234.

[36] Viktor Miruchna, Robert Walter, David Lindlbauer, Maren Lehmann, Regine Von Klitzing, and Jörg Müller. 2015. Geltouch: Localized tactile feedback through thin, programmable gel. In *Proceedings of the 28th Annual ACM Symposium on User Interface Software & Technology*. 3–10.

[37] Hila Mor, Tianyu Yu, Ken Nakagaki, Benjamin Harvey Miller, Yichen Jia, and Hiroshi Ishii. 2020. Venous Materials: Towards Interactive Fluidic Mechanisms. In *Proceedings of the 2020 CHI Conference on Human Factors in Computing Systems*. 1–14.

[38] Yuki Mori and Takeo Igarashi. 2007. Plushie: an interactive design system for plush toys. In *ACM SIGGRAPH 2007 papers*. 45–es.

[39] DuPont Teijin Films. Mylar. [n.d.]. http://usa.dupontteijinfilms.com/wp-content/uploads/2017/01/Mylar_Physical_Properties.pdf

[40] Kenichi Nakahara, Koya Narumi, Ryuma Niiyama, and Yoshihiro Kawahara. 2017. Electric phase-change actuator with inkjet printed flexible circuit for printable and integrated robot prototyping. In *2017 IEEE International Conference on Robotics and Automation (ICRA)*. IEEE, 1856–1863.

[41] Ryosuke Nakayama, Ryo Suzuki, Satoshi Nakamaru, Ryuma Niiyama, Yoshihiro Kawahara, and Yasuaki Kakehi. 2019. MorphIO: Entirely Soft Sensing and Actuation Modules for Programming Shape Changes through Tangible Interaction. In *Proceedings of the 2019 on Designing Interactive Systems Conference*. 975–986.

[42] Sasha M Novack, Eric Acome, Christoph Keplinger, Mirela Alistar, Mark D Gross, Carson Bruns, and Daniel Leithinger. 2021. Electriflow: Soft Electrohydraulic Building Blocks for Prototyping Shape-changing Interfaces. In *Designing Interactive Systems Conference 2021*. 1280–1290.

[43] Jifei Ou, Mélina Skouras, Nikolaos Vlavianos, Felix Heibeck, Chin-Yi Cheng, Jannik Peters, and Hiroshi Ishii. 2016. aeroMorph-heat-sealing inflatable shape-change materials for interaction design. In *Proceedings of the 29th Annual Symposium on User Interface Software and Technology*. 121–132.

[44] Ron Pelrine, Roy D Kornbluh, Qibing Pei, Scott Stanford, Seajin Oh, Joseph Eckerle, Robert J Full, Marcus A Rosenthal, and Kenneth Meijer. 2002. Dielectric elastomer artificial muscle actuators: toward biomimetic motion. In *Smart Structures and Materials 2002: Electroactive polymer actuators and devices (EAPAD)*, Vol. 4695. International Society for Optics and Photonics, 126–137.

[45] Jesús Pérez, Miguel A Otaduy, and Bernhard Thomaszewski. 2017. Computational design and automated fabrication of kirchhoff-plateau surfaces. *ACM Transactions on Graphics (TOG)* 36, 4 (2017), 1–12.

[46] Isabel P. S. Qamar, Rainer Groh, David Holman, and Anne Roudaut. 2018. *HCI Meets Material Science: A Literature Review of Morphing Materials for the Design of Shape-Changing Interfaces.* Association for Computing Machinery, New York, NY, USA, 1–23. https://doi.org/10.1145/3173574.3173948

[47] Mark Schenk and Simon D Guest. 2011. Origami folding: A structural engineering approach. *Origami* 5 (2011), 291–304.

[48] DuPont Teijin Films. Material Safety Data Sheet. [n.d.]. http://web.mit.edu/rocketteam/www/usli/MSDS/Mylar.pdf

[49] Jonathan Richard Shewchuk. 1996. Triangle: Engineering a 2D quality mesh generator and Delaunay triangulator. In *Workshop on Applied Computational Geometry*. Springer, 203–222.

[50] Emmanuel Siéfert, Etienne Reyssat, José Bico, and Benoît Roman. 2019. Bio-inspired pneumatic shape-morphing elastomers. *Nature materials* 18, 1 (2019), 24–28.

[51] Alexa F. Siu, Eric J. Gonzalez, Shenli Yuan, Jason B. Ginsberg, and Sean Follmer. 2018. *ShapeShift: 2D Spatial Manipulation and Self-Actuation of Tabletop Shape Displays for Tangible and Haptic Interaction.* Association for Computing Machinery, New York, NY, USA, 1–13. https://doi.org/10.1145/3173574.3173865

[52] Laura Stiles, Hanspeter Schaub, Kurt Maute, and Daniel Moorer. 2010. Electrostatic inflation of membrane space structures. In *AIAA/AAS Astrodynamics Specialist Conference*. 8134.

[53] Ltd. ATN Film SUNGMOON Electronics Co. [n.d.]. http://en.smec-korea.co.kr/product/pet.asp

[54] Ryo Suzuki, Ryosuke Nakayama, Dan Liu, Yasuaki Kakehi, Mark D. Gross, and Daniel Leithinger. 2020. LiftTiles: Constructive Building Blocks for Prototyping Room-Scale Shape-Changing Interfaces. In *Proceedings of the Fourteenth International Conference on Tangible, Embedded, and Embodied Interaction* (Sydney NSW, Australia) *(TEI '20)*. Association for Computing Machinery, New York, NY, USA, 143–151. https://doi.org/10.1145/3374920.3374941

[55] Yasaman Tahouni, Isabel PS Qamar, and Stefanie Mueller. 2020. NURBSforms: A Modular Shape-Changing Interface for Prototyping Curved Surfaces. In *Proceedings of the Fourteenth International Conference on Tangible, Embedded, and Embodied Interaction*. 403–409.

[56] Atieh Talebzadeh, Abhishek Patnaik, Xu Gao, and David E Swenson. 2015. Dependence of ESD charge voltage on humidity in data centers: Part II-Data analysis. *ASHRAE Transactions* 121 (2015), 37.

[57] Yichao Tang, Gaojian Lin, Shu Yang, Yun Kyu Yi, Randall D Kamien, and Jie Yin. 2017. Programmable Kiri-Kirigami Metamaterials. *Advanced Materials* 29, 10 (2017), 1604262.

[58] Ye Tao, Youngwook Do, Humphrey Yang, Yi-Chin Lee, Guanyun Wang, Catherine Mondoa, Jianxun Cui, Wen Wang, and Lining Yao. 2019. Morphlour: Personalized flour-based morphing food induced by dehydration or hydration method. In *Proceedings of the 32nd Annual ACM Symposium on User Interface Software and Technology*. 329–340.

[59] Søren Toxvaerd and Jeppe C Dyre. 2011. Communication: Shifted forces in molecular dynamics.

[60] Udayan Umapathi, Patrick Shin, Ken Nakagaki, Daniel Leithinger, and Hiroshi Ishii. 2018. Programmable droplets for interaction. In *Extended Abstracts of the 2018 CHI Conference on Human Factors in Computing Systems*. 1–1.

[61] Guanyun Wang, Tingyu Cheng, Youngwook Do, Humphrey Yang, Ye Tao, Jianzhe Gu, Byoungkwon An, and Lining Yao. 2018. Printed paper actuator: A low-cost reversible actuation and sensing method for shape changing interfaces. In *Proceedings of the 2018 CHI Conference on Human Factors in Computing Systems*. 1–12.

[62] Wen Wang, Lining Yao, Teng Zhang, Chin-Yi Cheng, Daniel Levine, and Hiroshi Ishii. 2017. *Transformative Appetite: Shape-Changing Food Transforms from 2D to 3D by Water Interaction through Cooking.* Association for Computing Machinery,

New York, NY, USA, 6123–6132. https://doi.org/10.1145/3025453.3026019

[63] Paul K Weiner, Robert Langridge, Jeffrey M Blaney, Ronald Schaefer, and Peter A Kollman. 1982. Electrostatic potential molecular surfaces. *Proceedings of the National Academy of Sciences* 79, 12 (1982), 3754–3758.

[64] Craig Wisneski, Hiroshi Ishii, Andrew Dahley, Matt Gorbet, Scott Brave, Brygg Ullmer, and Paul Yarin. 1998. Ambient displays: Turning architectural space into an interface between people and digital information. In *International Workshop on Cooperative Buildings*. Springer, 22–32.

[65] Lining Yao, Ryuma Niiyama, Jifei Ou, Sean Follmer, Clark Della Silva, and Hiroshi Ishii. 2013. PneUI: pneumatically actuated soft composite materials for shape changing interfaces. In *Proceedings of the 26th annual ACM symposium on User interface software and Technology*. 13–22.

[66] Lining Yao, Jifei Ou, Chin-Yi Cheng, Helene Steiner, Wen Wang, Guanyun Wang, and Hiroshi Ishii. 2015. bioLogic: Natto cells as nanoactuators for shape changing interfaces. In *Proceedings of the 33rd Annual ACM Conference on Human Factors in Computing Systems*. 1–10.